PROCEEDINGS OF SPIE

SPIEDigitalLibrary.org/conference-proceedings-of-spie

Far-infrared/submillimeter imager-polarimeter using distributed antenna-coupled transition edge sensors

Peter K. Day, Henry G. LeDuc, Alexey Goldin, Charles Darren Dowell, Jonas Zmuidzinas

Peter K. Day, Henry G. LeDuc, Alexey Goldin, Charles Darren Dowell, Jonas Zmuidzinas, "Far-infrared/submillimeter imager-polarimeter using distributed antenna-coupled transition edge sensors," Proc. SPIE 5498, Millimeter and Submillimeter Detectors for Astronomy II, (8 October 2004); doi: 10.1117/12.552440

SPIE.

Event: SPIE Astronomical Telescopes + Instrumentation, 2004, Glasgow, United Kingdom

Far Infrared/ Submillimeter Imager-Polarimeter Using Distributed Antenna-Coupled Transition Edge Sensors

Peter K. Day[a], Henry LeDuc[a], Alexey Goldin[a], C. Darren Dowell[a] and Jonas Zmuidzinas[b]

[a]Jet Propulsion Laboratory, California Institute of Technology, Pasadena, CA 91109;
[b]California Institute of Technology, Pasadena, CA 91125

ABSTRACT

We describe a new concept for a detector for the submillimeter and far infrared that uses a *distributed* hot–electron transition edge sensor (TES) to collect the power from a focal–plane–filling slot antenna array. Because superconducting transmission lines are lossy at frequencies greater than about 1 Thz, the sensors must directly tap the antenna, and therefore must match the antenna impedance ($\sim$ 30 ohms). Each pixel contains many TESs that are all wired in parallel as a single distributed TES, which results in a low impedance that can match to a multiplexed SQUID readout. These detectors are inherently polarization sensitive, with very low cross–polarization, but can also be easily configured to sum both polarizations for imaging applications. The single polarization version can have a very wide bandwidth of greater than 10:1 with a quantum efficiency greater than 50%. The dual polarization version is narrow band, but can have a higher quantum efficiency. The use of electron-phonon decoupling obviates the need for micro–machining, making the focal plane much easier to fabricate than with absorber–coupled, geometrically isolated pixels. An array of these detectors would be suitable for an imager for the Single Aperture Far Infrared (SAFIR) observatory. We consider two near–term applications of this technology, a 32×32 element imaging polarimeter for SOFIA and a 350μm camera for the CSO.

Keywords: bolometer, TES, detector array, slot antenna

1. INTRODUCTION

A key need exists for large arrays of detectors for imaging at FIR/Submillimeter wavelengths, especially using detectors with polarization sensitivity. The major technological barrier faced by existing array designs is the difficulty of fabricating the complicated micromachined structures that are involved and the fragility of these structures during bump–bonding to readout multiplexer chips. These difficulties are compounded as the designs for ground–based arrays are adapted to future space applications because the higher required sensitivities lead to even more fragile, difficult to fabricate structures. Our concept solves this critical problem by using an innovative pixel design, based on an antenna–coupled, *distributed* transition edge sensor (TES), operating in the hot–electron mode. We discuss this new pixel design and present the results of thermal conductance measurements which confirm the viability of our concept.

The transition edge sensor with electrothermal feedback[1,2] is a leading candidate detector technology for astronomical imaging applications from millimeter wavelengths to X–rays. Interest in TES arrays is complemented by developments in the area of SQUID multiplexers,[3,4] which reduce the number of wires needed to read out a large array, and by the ability to fabricate arrays using lithographic methods, rather than by manual assembly as required with germanium detectors. At FIR through millimeter wavelengths, detectors are commonly based on a thermally isolated absorbing wire grid or resistive layer with sheet resistance matched to the impedance of free space. In order to obtain high absorbtion efficiency, a quarter–wavelength backshort can be used, which also limits the bandwidth of the detector to about an octave.

Arrays of detectors based on absorber–coupled pixels with direct readout (*i. e.* not multiplexed) semiconducting sensors are used in current state–of–the–art instruments. The Submillimeter High Angular Resolution Camera II (SHARC-II)[5,6] employs a filled array of 384 absorber–coupled doped silicon detectors using the "pop–up–detector" architecture. Bolocam[7] is a 144–element feed-horn coupled array using "spider–web" bolometers

Further author information: (Send correspondence to P.K.D.)
P.K.D: E-mail: Peter.K.Day@jpl.nasa.gov, Telephone: 626 577 5582

Millimeter and Submillimeter Detectors for Astronomy II, edited by
Jonas Zmuidzinas, Wayne S. Holland, Stafford Withington, Proceedings of
SPIE Vol. 5498 (SPIE, Bellingham, WA, 2004) · 0277-786X/04/$15 · doi: 10.1117/12.552440

with germanium detectors. In order to realize a significant gain in instrument sensitivity, arrays of at least 1000 elements are needed, which dictates a purely lithographic process utilizing TES bolometers and no manual assembly. SCUBA-II, which uses a $\sim 10^4$ pixel array of absorber–coupled TES bolometers, is an attempt to take this next step, but faces a challenging fabrication effort.

The 2001 Decadal Report issued by the National Academy of Science endorsed the Single Aperature Far–Infrared Observatory (SAFIR) mission as a priority for study in this decade and operation in the next. SAFIR will explore the universe from 50 to 500 microns and will require an array with approximately 128×128 detectors with noise equivalent power (NEP) of around $10^{-18}\mathrm{W}/\mathrm{Hz}^{1/2}$ to be photon noise limited. As pathfinders for the SAFIR mission, suborbital instruments should employ detector technologies that are scalable to the space mission's requirements. For geometrically isolated, absorber–coupled pixels, this means reducing the thermal conductance, G, of the structural supports *by three orders of magnitude* to get from the SCUBA-II value of 3×10^{-17} to $\sim 10^{-18}\mathrm{W}/\mathrm{Hz}^{1/2}$.

Clearly, a more advanced pixel architecture would be desirable. In the area of millimeter–wave detectors, advanced pixel designs incorporating antenna–coupled TES bolometers have been proposed and demonstrated.[8,9] In these devices, power from a planar antenna is transmitted down a transmission line to a load resistor, which is thermally isolated on a small island along with a TES. Antenna–coupled pixels have several important advantages. First, only the load resistor and TES need to be thermally isolated, so the micromachined structures are much simpler. Second, the specific heat of the absorber is avoided, so the detectors can be much faster. Third, the bandwidth can be made greater than with an aborber plus 1/4–wave backshort combination by using a suitably broad-band antenna. No backshort is needed as the antenna lies on a substrate with high dielectric constant, so most of the power is radiated into the substrate (hence, most of the power incident on the antenna through the substrate can be efficiently absorbed). The millimeter–wave antenna–coupled devices have additional benefits: phased array antennas can be used that have narrow beam widths that couple easily to a telescope, and filters can be inserted in the microstrip transmission line between antenna and TES to define the pass–band.

While microstrip coupling to antennas is a powerful technique for millimeter–wave detectors, for frequencies above about 700 Ghz, the gap frequency of niobium, the superconducting transmission lines become lossy and can no longer transmit power over the required distances ($\sim \lambda$). For FIR/Submillimeter detectors, antenna–coupled designs have been proposed with the sensor collocated with the antenna,[10,11] where the power collected by the antenna is dissipated directly in the TES. The normal resistance of the TES must be matched to the antenna impedance for efficient absorption. In these devices, thermal isolation is achieved through the thermal decoupling of the electrons and phonons in the TES, *ie.* the "hot electron" effect. The athermal electrons can be confined to the TES through Andreev reflection if the contacts are made of a superconducting material with a large gap parameter, Δ. The thermal conductance is then proportional to the volume of the sensor, prescribing a very small TES volume for low enough G. One drawback of this sort of detector is that the TES normal resistance must be at least 30Ω in order to match to the antenna impedance. Such a large resistance does not match well to a SQUID readout, as for a given bias power, P_{bias}, the contribution to the NEP from the SQUID current noise,

$$\mathrm{NEP}_{\mathrm{SQUID}} = \delta I_{\mathrm{SQUID}} \sqrt{R_{\mathrm{TES}} P_{\mathrm{bias}}} \tag{1}$$

increases with the square root of the TES resistance. For non-multiplexed readout, the SQUID noise can be made low enough, but multiplexers incur a noise penalty of $\sqrt{M}$ in the noise of the front end SQUID, where M is the multiplexing factor, making resistances greater than a few hundreds of milliohms incompatible with that technology. A variant of the hot–electron antenna–coupled detector has been proposed[12] where the antenna power is dissipated in a resistor and the resulting hot electrons diffuse into a separate low–resistance TES. The challenge for this "composite" detector concept is to engineer the structure to achieve efficient coupling with a sufficiently small device volume to achieve the desired sensitivity.

Another drawback of the simple hot–electron antenna–coupled detector is that the active area of the antenna is much smaller than the pixel size, which is $kf\lambda$ for a given f/number. For Nyquist sampling, $k = 0.5$. Hence, to efficiently fill the focal plane, an aperture–defining dielectric lens must be placed in front of each antenna.

2. DEVICE CONCEPT

The new antenna–coupled pixel concept we describe leads to a filled focal plane without the need for lenses or feedhorns and is compatible with SQUID multiplexing. In addition, large arrays are robust and straight forward to fabricate. The layout of an individual pixel is shown in fig. 1. As with millimeter–wave slot array antennas, an array of slots in a ground plane filling the desired pixel area make up an antenna. In contrast to the millimeter–wave case, the antenna is periodically tapped directly by an array of transition–edge hot–electron microbolometers, which absorb the power from the antenna. Each microbolometer is shorted to one side of the slot and attached to a capacitor on the other side that constitutes an RF short at the antenna frequency. In the case of a single polarization device, an array of long slots is used, where the spacing between slots, δ_s satisfies $\delta_s < \lambda/\sqrt{\epsilon_r}$ to preclude surface waves[9], where ϵ_r is the relative dielectric constant of the substrate (fig. 1a). The same condition applies for the spacing between the microbolometers along the slots. For $f/4$ and a silicon substrate ($\epsilon_r = 11.6$), the number of microbolometers is approximately 64 for $k = 0.5$ and 256 for $k = 1$. The microbolometers for a pixel are all wired in parallel, and the current through the parallel combination is measured with a SQUID using the standard voltage–biased TES readout circuit (fig. 1d). The power absorbed by the microbolometers is thus combined incoherently in contrast with the millimeter–wave device[9] where coherent addition is accomplished with microstrip lines. The beam pattern from the pixel will be broad like that of a single slot antenna, which has a beam pattern comparable to that of an absorbing wire–grid. The dual polarization version of the device is shown in fig.1b. In that case, both vertical and horizonal slots are used. The signals from the two polarizations may be read independently on separate channels, or they may be combined on-pixel.

Whereas the resistance of each microbolometer is designed to be about 30Ω to match to the antenna, the resistance of the parallel combination of N such elements is in the range of 100 to 400mΩ, depending on the number of microbolometers per pixel. The lower end of this range is compatible with the present version of the SQUID multiplexer developed by the NIST group,[3] and it is believed to be compatible with the multiplexer being developed at Berkeley.[4] The voltage bias of the circuit results in stable operation of the parallel combination of microbolometers, which is topologically equivalent to a single sensor with N times the volume. If one bolometer falls in temperature, the local joule heating increases and the bolometer tends to warm back to its individual T_c. For electron–phonon decoupling the thermal conductance is proportional to the total volume of the sensor. The thermal noise is

$$\mathrm{NEP}_{\mathrm{thermal}} = \sqrt{4k_B T^2 G}, \tag{2}$$

so the NEP of an individual microbolometer would be $\sqrt{N}$ times smaller than the combination if it were biased separately.

The calculated antenna efficiencies for the single–polarization (long slots, fig. 1a) and dual–polarization (cross slots, fig. 1b) versions of the detector are shown in fig. 2. The calculation was done using the method–of–moments. The single–polarization version has a *very wide bandwidth of greater than 10:1*, limited on the long wavelength side by the length of the slots and on the short wavelength side by the spacing of the microbolometers. With the dual–polarization version, the bandwidth is limited to about 30% because the slots must be broken in order to be able to run the wiring out to the sides of the pixel. These calculated efficiencies only consider the matching between the antenna and bolometers. The actual efficiency is lower because only part of the power "radiated" by the antenna is directed into the substrate (toward the telescope). The other part is radiated into the vacuum behind the focal plane. The power division ratio is approximately $\sqrt{\epsilon_r} : 1$, giving an efficiency of about 71% for a silicon substrate. We assume that the illuminated side of the substrate has a suitable antireflection coating. With the narrow–band dual–polarization devices, it would be possible to use a 1/4–wavelength resonant substrate, in which case the power division ratio is $\epsilon_r : 1$ (about 90% efficiency). A further reduction in efficiency comes from the fact that the ground plane of the antenna is slightly lossy at submillimeter/FIR frequencies. Use of a high conductivity metal, such as gold or epitaxial niobium, will minimize this effect. With a normal metal, a niobium contact region between the bolometer and the groundplane would be required so that the hot electrons would be confined to the bolometer through Andreev reflection. Groundplane losses will be calculated in more detail, but are expected to be only a few percent.

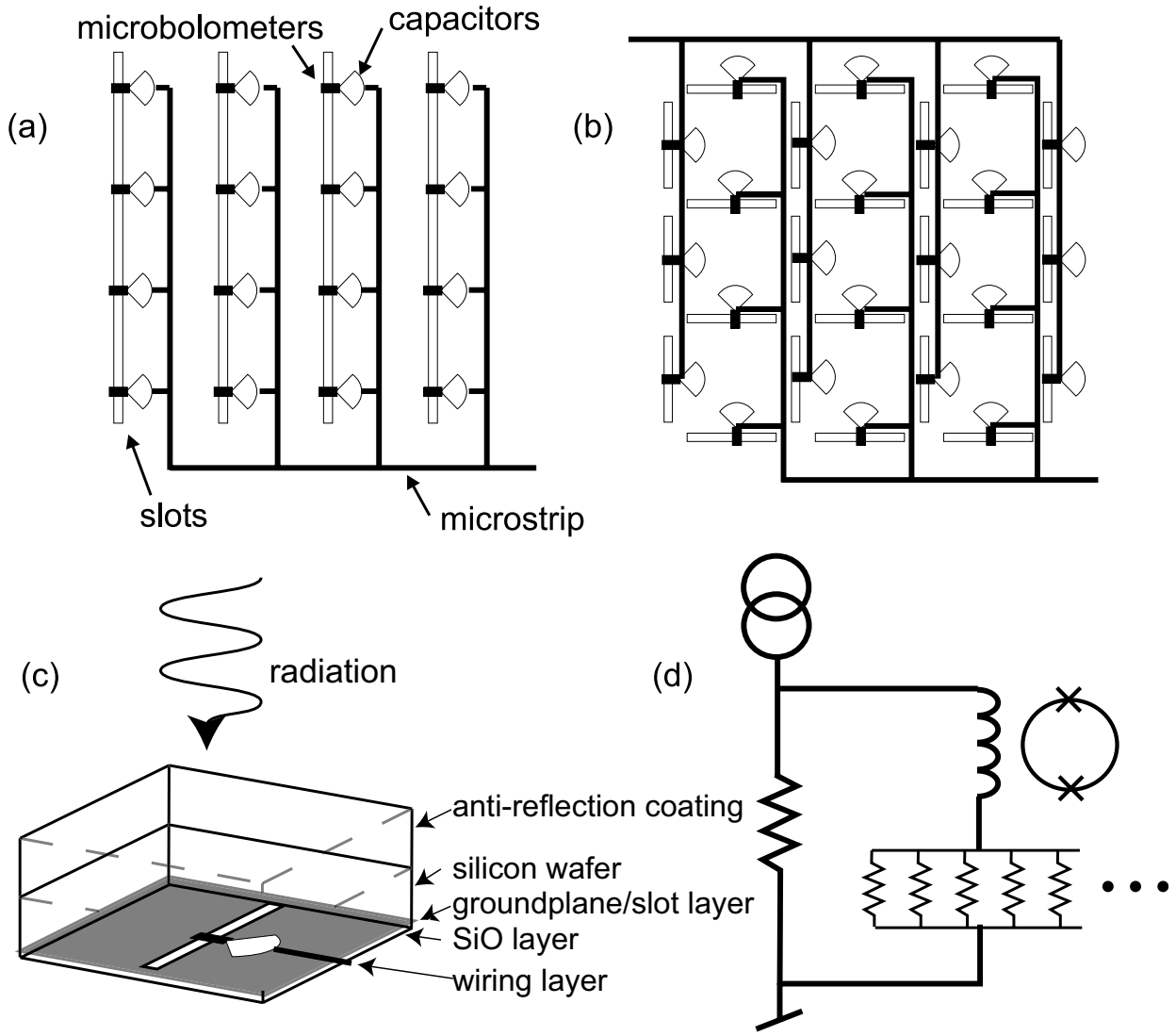

Figure 1. The distributed antenna–coupled FIR/Submm pixel. (a) Single polarization version. An array of long parallel slots in a groundplane is periodically tapped by an array of microbolometers. For clarity only 16 bolometers are depicted, whereas an actual device will have between 64 and 256. The DC bias for the microbolometers is supplied via the microstrip lines, and the return current path is through the groundplane. (b) Dual polarization version with separate readouts for the two polarizations. (c) The pixel is illuminated through the dielectric substrate. An antireflection coating is used to increase the quantum efficiency. (d) The individual microbolometers are wired in parallel and voltage biased. The current through the parallel combination is monitored with a SQUID ammeter.

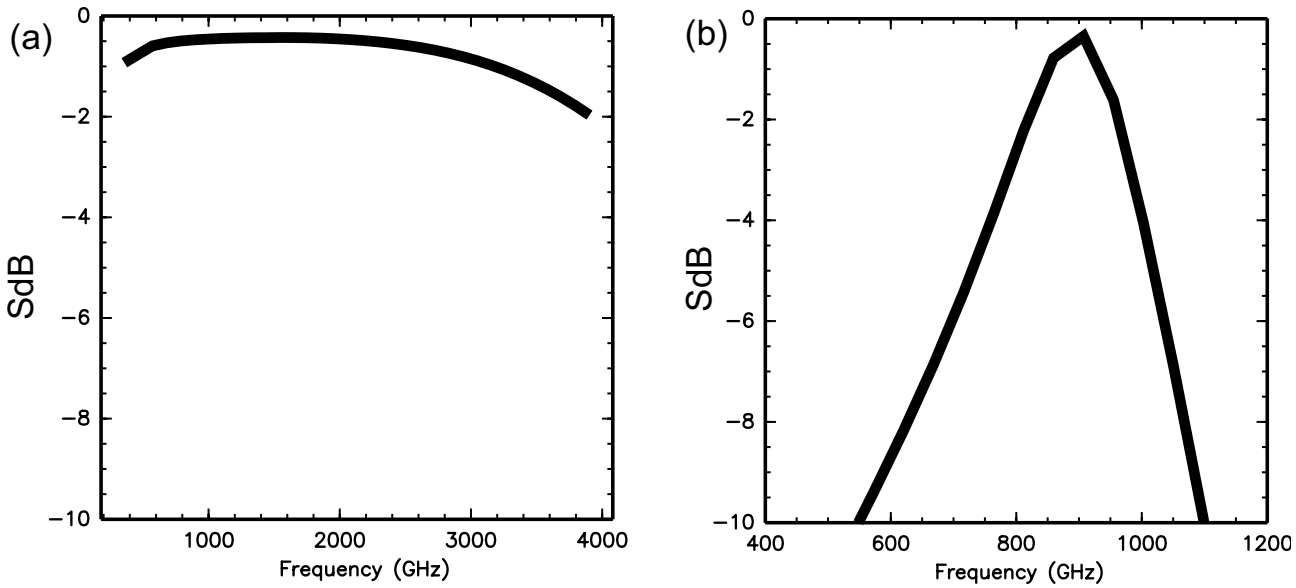

Figure 2. (a) Antenna efficiency of the single–polarization detector, with 45Ω microbolometers (b) Efficiency for the dual polarization detector. The antennas are slots of 64μm length 2μm width. The period is 74 μm and the 30Ω microbolometers are offset by 26μm from the slot centers.

3. MEASUREMENTS

To test the feasibility of our concept, we performed measurements on a parallel combination of 64 microbolometers, each 1μm on a side, made from a 200$\mathring{A}$ thick titanium film with a transition temperature of 140mK. The resistance of each microbolometer was 54Ω, slightly larger than the target value but in the range that is appropriate for antenna coupling, and that of the parallel combination was 0.85Ω. The readout circuit of fig. 1(d) was used. Figure 3(a) shows measurements of the total bias power versus parallel resistance at different bath temperatures. These bias curves are characteristic of a single TES and demonstrate that the distributed device *does* act as a single bolometer. The slope of the curves indicates that the transition is rather broad, about 20mK from top to bottom. We ascribe the broadness to the quality of the film, and believe that refinements can lead to somewhat sharper transitions. Very sharp transitions are not needed for submillimeter detection, although a very broad transition will reduce the efficiency of the detector. By plotting device power versus bath temperature for fixed TES resistance, information about the electron–phonon thermal conductance is obtained (fig. 3b). We find that for $T_c = 140$mK, the total G is 14 pW/K. For the same device volume and $T_c = 100$mK, the calculated $\mathrm{NEP_{thermal}} = 2 \times 10^{-18}\mathrm{W}/\mathrm{Hz}^{1/2}$. The noise can be further lowered by reducing the sensor volume, either by using thinner films or reducing the lateral dimensions; *but these data show that the NEP required for SAFIR is achievable using this pixel architecture.*

For ground–based and airborne applications FIR/Submillimeter detectors become photon-noise limited at $\mathrm{NEP} \sim 10^{-16}\mathrm{W}/\mathrm{Hz}^{1/2}$. For these applications the transition temperature of the microbolometers may be raised to ease cooling requirements. Theoretically for electron–phonon decoupling,[13] G scales with temperature as T^4. From eqn. 2, we can expect that NEP scales as T^3. Based on the measured noise of our present device, we obtain NEPs of 2.5×10^{-17} and 6×10^{-17} for transition temperatures of 0.3 and 0.4K, respectively.

Unfortunately, the time constant of a hot–electron TES thermistor becomes quite fast at temperatures much higher than about 100mK. Current SQUID multiplexers cannot read out a very fast thermistor without adding extra noise. For stable biasing, the electrical time constant of the bias circuit must be at least a factor of 6 smaller than the thermistor's thermal time constant. In the case of the time division SQUID multiplexer, the noise appearing inside the electrical bandwidth must be Nyquist sampled. The settling times of the various stages of the multiplexer circuit set a limit on sample rate that can be realized, which translates back to a

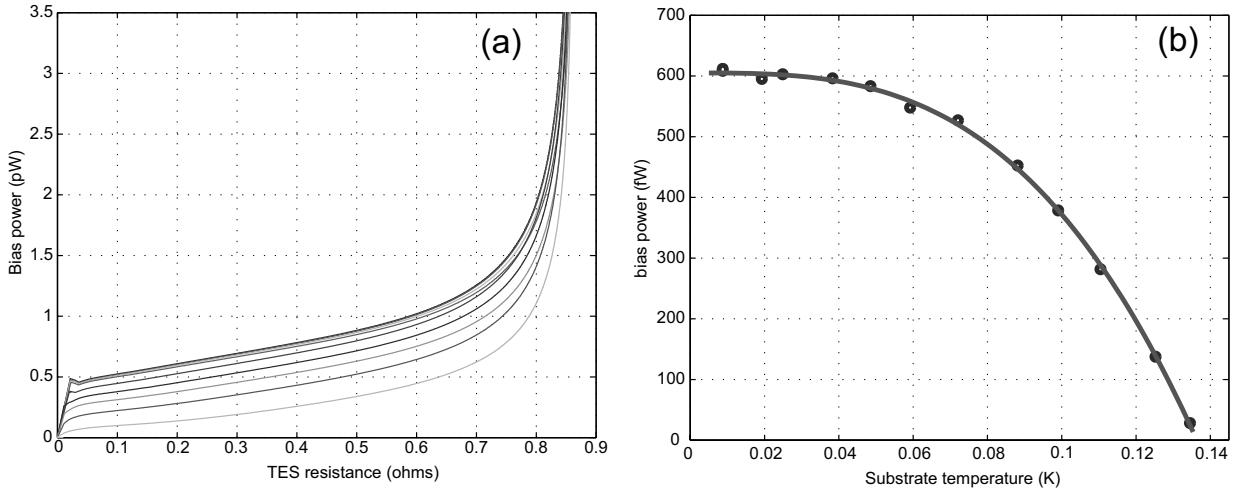

Figure 3. (a) Bias curves measured at varying bath temperatures for 64 $1\mu\text{m}^2$ titanium microbolometers wired in parallel. (b) Derived bias power versus bath temperature for a resistance of 0.2Ω.

lower limit on the thermistor's time constant, roughly in the range of $100\mu s$ to 1ms, depending on the level of cross-talk rejection required. Improvements to the bandwidth of this type of multiplexer which may lead to a factor of 4 improvement in sample rate have been identified.[14] A similar bandwidth limitation applies to the frequency division multiplexer. In that case, the sensor noise appears as a sideband on each of the bias frequencies, which must then be separated by more than the sensor bandwidth to avoid overlap. For a given SQUID system bandwidth, the sensor time constant determines the number of pixels that can be multiplexed.

To keep the thermistor's time constant low, the detectors must be operated at around 100mK. At low temperature, the electron–phonon thermal conductance in the titanium film is described by the "dirty" limit, $q_T l \ll 1$, where q_T is the wavenumber of a thermal phonon, and l is the electron mean free path.[15] In that limit, the electron–phonon relaxation rate, τ_{e-ph}, varies as $\tau_{e-ph}^{-1} \propto T^4 l$, and is suppressed relative to the clean limit. Relaxation times of 10^{-3}s have been measured at 100mK for thin titanium and halfnium films.[16] The relaxation time of the microbolometer will be longer than the normal metal τ_{e-ph} by about a factor of two because of the electronic heat capacity enhancement at the superconducting transition temperature, but will be shortened by electro–thermal feedback. The speed–up factor will be kept low because the very small sensors tend to have relatively broad transitions, hence weak electo–thermal feedback.

The pixels of our new design can be easily assembled into a focal plane. An advantage of the use of slot antennas is that is that the wiring for the readout may be "hidden" behind the groundplane. There is ample space to run the wiring out to the sides of the array using microstrip lines routed between the pixels. One wire is required per pixel as the return currents flow through the groundplane. For a 1 mm pixel side length, the distance between slots may be between 62 and 125μm, depending on the number of slots per pixel. For a 1.5 μm linewidth and 1.5 μm gaps, the space required to bring out the wiring for a column of 16 pixels is only 48 μm. Arranging the array in four two–side–buttable quadrants of 16×16, we can see that for a single polarization 32×32 array *essentially 100% filling factor may be realized*. For a dual polarization array, where the horizontal slots leave smaller gaps, about 5% of the focal plane area will be consumed by the wiring streets for the same array format. At the sides of the array, bump–bonding may be used to make contact to a SQUID multiplexer chip. Because no micromachining has been used, the bump–bonding is straight–forward. Larger arrays may be wired in the same manner using either thinner wires or multiple wiring layers.

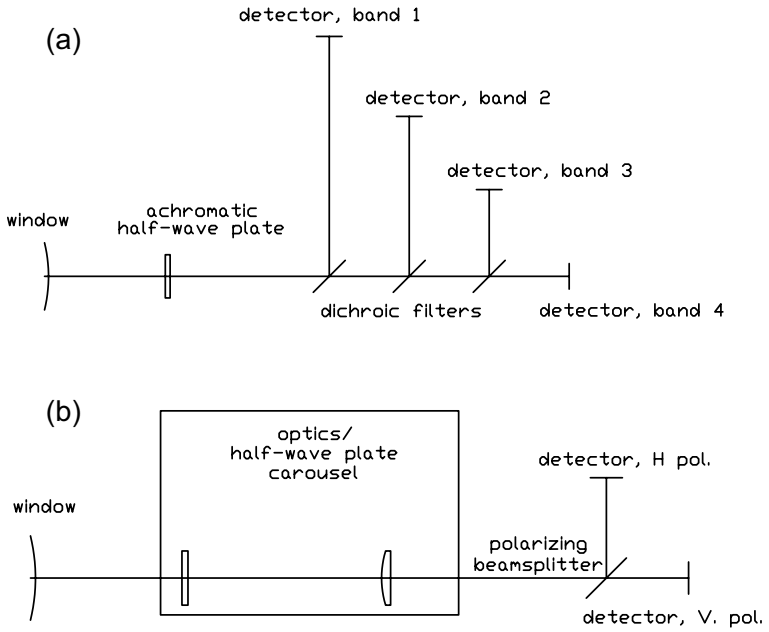

Figure 4. Schematic optical designs for a multi–band SOFIA imaging polarimeter using dual–polarization (a) or single–polarization (b) detector arrays. Due to the relatively small bandwidth of the dual–polarization detectors, one array is needed for each far–IR band. These arrays could provide simultaneous multi–color imaging of a source with dichroic filters and an achromatic modulator. The broad–bandwidth, single polarization arrays allow an arbitrary number of wavelength bands, selected by filter/lens/half–wave plate mechanisms. Two arrays and a polarizing beamsplitter are needed to recover all of the radiation in the field of view.

4. APPLICATIONS

4.1. Far–Infrared Polarimeter Array for SOFIA

SOFIA, which should begin flights in 2004, reopens the far-infrared (30 - 300 μm) sky to new detector technology in receivers fielded on the timescale of 2-3 years. SOFIA has an accurate 2.5 m primary mirror which achieves $10''$ resolution at $\lambda = 100$ μm. The shorter wavelengths of the far-IR range are covered by photon-counting arrays. However, bolometer arrays are a good choice for $\lambda > 100$ μm since they offer high quantum efficiency. The first-light far-IR camera for SOFIA, called HAWC, will have a 12×32 array of semiconducting bolometers with 50% quantum efficiency, using an unmultiplexed technology which is difficult to scale to larger formats. We propose to develop a background–limited 32×32 detector suitable for SOFIA with a quantum efficiency at least this high. In particular, we are pursuing a multiband imaging ($\Delta\lambda/\lambda = 0.1$) array with polarization sensitivity that could be used in a polarimeter/second-generation camera. An instrument which detects both states of linear polarization independently has the same sensitivity per beam when operating as a camera as an instrument without polarization sensing.

A polarimeter on SOFIA will have the resolution and sensitivity to cross new threshholds in the measurement of magnetic field structures of envelopes and disks surrounding (proto)stars and the Galactic center; the far-IR range is particularly important in identifying the the fields in different spatial components in the case that they have different dust temperatures. The proposed polarimeter would make among the first measurements of magnetic field structures in the dense interstellar medium of nearby galaxies and, in the case of a large field of view (at least 32 detectors across at one of the longer wavelength bands) would likely detect magnetic field orientations in bright patches of infrared cirrus in our own Galaxy. We would also be uniquely equipped to study the wavelength dependence of polarization from the interstellar medium and could provide maps of magnetic fields with significant spatial dynamic range suitable for studies of turbulence.

A pixel scale of ∼1 mm is readily accommodated in a SOFIA far-IR instrument. In the case of the dual

polarization detectors, we will need a detector array for each of the ∼4 bands we wish to cover. With dichroic filters and an achromatic polarization modulator in front of the focal plane, it is possible to measure intensity and polarization in several wavelength bands simultaneously (fig. 4a). A polarimeter/imager could also effectively employ the single-polarization/broad bandwidth detector arrays. To achieve full sensitivity per beam, this detector design necessitates the use of a polarizing beam splitter and a pair of detector arrays. However, the number of detectors and readouts necessary to cover ∼4 wavelength bands is minimized since the same detector arrays can be used for each band (fig. 4b). (Of course, with greater cost and complexity, one could also implement the dichroic multiband configuration.)

At far-IR wavelengths, polarization modulation for large (even 64×64) arrays is still managed easily with traditional rotating half-wave plates.

4.2. Ground–Based Submillimeter Camera

There is motivation to field a $\sim 32 \times 32$ TES array on a ground-based submillimeter telescope such as the Caltech Submillimeter Observatory. The state-of-the art 350 μm camera SHARC II (12×32) and 450/850 μm camera SCUBA (91 + 37 detector) are both capable of detecting high-redshift galaxies of known position in a reasonable integration time, but are inefficient at surveying blank fields for submillimeter-selected sources. A jump in field of view by a factor of a few is enough to generate statistically significant samples in surveys. Large arrays will also make possible the mapping of many nearby normal spiral galaxies as well as entire galactic molecular clouds. Undoubtedly, SCUBA-2 will make significant inroads into these areas of research; our proposed camera would provide similar mapping capability to the U.S. community. If we choose to instrument a polarimeter with the submillimeter TES array, we would also make an order of magnitude leap in the speed of mapping submillimeter polarization.

REFERENCES

1. K.D. Irwin. An application of electrothermal feedback for high-resolution cryogenic particle-detection. *Appl. Phys. Lett.*, 66(15):1998–2000, 1995.
2. A.T. Lee, P.L. Richards, S.W. Nam, B. Cabrera, and K.D. Irwin. A superconducting bolometer with strong electrothermal feedback. *Appl. Phys. Lett.*, 69(12):1801–1803, 1996.
3. J.A. Chervenak, K.D. Irwin, E.N. Grossman, J.M. Martinis, C.D. Reintsema, and M.E. Huber. Superconducting multiplexer for arrays of transition edge sensors. *Appl. Phys. Lett.*, 74(26):4043–4045, 1999.
4. J. Yoon, J. Clarke, J.M. Gildemeister, A.T. Lee, M.J. Myers, P.L. Richards, and J.T. Skidmore. Single superconducting quantum interference device multiplexer for arrays of low-temperature sensors. *Appl. Phys. Lett.*, 78(3):371–373, 2001.
5. G. M. Voellmer, C. A. Allen, M. J. Amato, S. R. Babu, A. E. Bartels, D. J. Benford, R. J. Derro, C. D. Dowell, D. A. Harper, M. D. Jhabvala, S. H. Moseley, T. Rennick, P. J. Shirron, and J. G. Staguhn. Design and fabrication of two–dimensional semiconducting bolometer arrays for the high–resolution airborne wideband camera (hawc) and the submillimeter high angular resolution camera II (SHARC-II). *Proc. SPIE*, 4855:63–72, 2002.
6. C. D. Dowell, C. A. Allen, S. R. Babu, M. M. Freund, M. B. Gardner, J. Groseth, M. D. Jhabvala, A. Kovacs, D. C. Lis, S. H. Moseley, T. G. Phillips, Silverberg R. F., G. M. Voellmer, and H. Yoshida. Sharc-II: A caltech submillimeter observatory facility camera with 384 pixels. *Proc. SPIE*, 4855:73–87, 2002.
7. J. Glenn, J. J. Bock, G. Chattopadhyay, S. F. Edgington, A. E. Lange, J. Zmuidzinas, P. D. Mauskopf, B. Rownd, L. Yuen, and P. A. R. Ade. Bolocam: a millimeter–wave bolometric camera. *Proc. SPIE*, 3354:326–334, May 2002.
8. C. L. Hunt, J. J. Bock, P. K. Day, A. Goldin, A. E. Lange, H. LeDuc, A. Vayonakis, and J. Zmuidzinas. Transition–edge superconducting antenna–coupled bolometer. *Proc. SPIE*, 3354:318–321, May 2002.
9. A. Goldin, J. J. Bock, C. Hunt, A. E. Lange, H. LeDuc, A. Vayonakis, and J. Zmuidzinas. Design of broadband filters and antennas for SAMBA. *Proc. SPIE*, 3354:163–171, May 2002.
10. M. Nahum and J. M. Martinis. Ultasensitive-hot-electron microbolometer. *Appl. Phys. Lett.*, 63(22):3075–3077, Nov 1993.

11. B. S. Karasik, W. R. McGrath, M. E. Gershenson, and A. V. Sergeev. Photon–noise–limited direct detector based on disorder–controlled electron heating. *J. Appl. Phys.*, 87(10):7586–7588, May 2000.
12. S. Ali, L. D. Cooley, D. McCammon, K. L. Nelms, J. Peck, D. Prober, D. Swetz, P. T. Timbie, and D. van der Weide. Planar antenna–coupled transition-edge hot electron microbolometer. *IEEE Trans. Applied Superconductivity*, 13(2):184–187, 2003.
13. B. Cabrera, R.M. Clarke, P. Colling, A.J. Miller, S. Nam, and R.W. Romani. Detection of single infrared, optical, and ultraviolet photons using superconducting transition edge sensors. *Appl. Phys. Lett.*, 73(6):735–737, 1998.
14. P.A.J. de Korte, J. Beyer, S. Deiker, G.C. Hilton, K.D. Irwin, M. Macintosh, S.W. Nam, C.D. Reintsema, L.R. Vale, and M.E. Huber. Time–division superconducting quantum interference device multiplexer for transition–edge sensors. *Rev. Sci. Inst.*, 74(8):3807, 2003.
15. A.V. Sergeev and V. Mitin. Electron–phonon interaction in disordered conductors: Static and vibrating scattering potentials. *Phys. Rev. B.*, 61(9):6041–6047, 2000.
16. M.E. Gershenson, D. Gong, T. Sato, B.S. Karasik, and A.V. Sergeev. Millisecond electron–phonon relaxation in ultrathin disordered metal films at millikelvin temperatures. *Appl. Phys. Lett.*, 79(13):2049–2051, 2001.